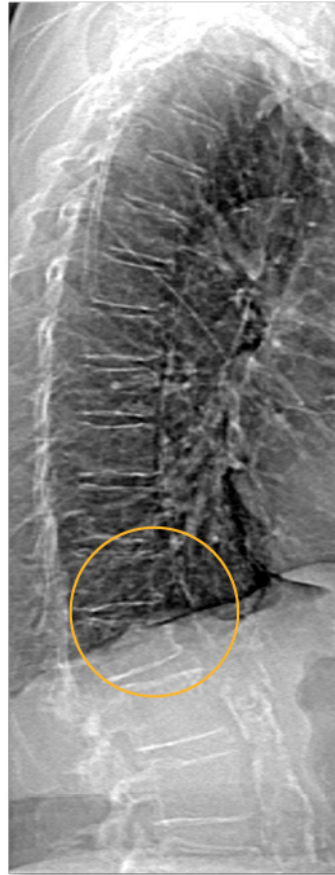


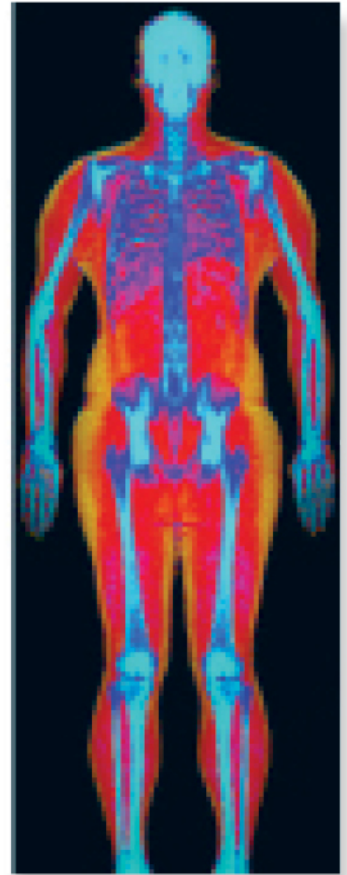
Powerful images. Clear answers.



Manage Patient's concerns about
Atypical Femur Fracture*



Vertebral Fracture Assessment –
a critical part of a complete
fracture risk assessment



Advanced Body Composition®
Assessment – the power to
see what's inside

Contact your Hologic rep today at BSHSalesSupportUS@hologic.com



PAID ADVERTISEMENT

*Incomplete Atypical Femur Fractures imaged with a Hologic densitometer, courtesy of Prof. Cheung, University of Toronto

ADS-02018 Rev 003 (10/19) Hologic Inc. ©2019 All rights reserved. Hologic, Advanced Body Composition, The Science of Sure and associated logos are trademarks and/or registered trademarks of Hologic, Inc., and/or its subsidiaries in the United States and/or other countries. This information is intended for medical professionals in the U.S. and other markets and is not intended as a product solicitation or promotion where such activities are prohibited. Because Hologic materials are distributed through websites, eBroadcasts and tradeshows, it is not always possible to control where such materials appear. For specific information on what products are available for sale in a particular country, please contact your local Hologic representative.

www.hologic.com | dxaperformance.com | 1.800.442.9892

Pathobiologic Mechanisms of Neurodegeneration in Osteopetrosis Derived From Structural and Functional Analysis of 14 *CLC-7* Mutants

Eleonora Di Zanni,¹ Eleonora Palagano,^{2,3} Laura Lagostena,¹ Dario Strina,^{2,3} Asma Rehman,⁴ Mario Abinun,^{5,6} Lien De Somer,⁷ Baldassarre Martire,⁸ Justin Brown,^{9,10} Ariana Kariminejad,¹¹ Shanti Balasubramaniam,¹² Gareth Baynam,^{13,14,15,16} Fiorella Gurrieri,¹⁷ Maria A Pisanti,¹⁸ Ilaria De Maggio,¹⁸ Miguel R Abboud,¹⁹ Robert Chiesa,²⁰ Christine P Burren,^{21,22} Anna Villa,^{2,23} Cristina Sobacchi,^{2,3}  and Alessandra Picollo¹ 

¹Consiglio Nazionale delle Ricerche, Istituto di Biofisica (CNR-IBF), Dulbecco Telethon Laboratory, Genoa, Italy

²Consiglio Nazionale delle Ricerche-Istituto di Ricerca Genetica e Biomedica (CNR-IRGB), Milan, Italy

³Humanitas Clinical and Research Center, Rozzano, Italy

⁴UMB Department of Biochemistry and Molecular Biology, University of Maryland, Baltimore, MD, USA

⁵Department of Pediatric Immunology, Great North Children's Hospital, Newcastle upon Tyne Hospitals NHS Foundation Trust, Newcastle upon Tyne, UK

⁶Translational and Clinical Research Institute, Faculty of Medical Sciences, Newcastle University, Newcastle upon Tyne, UK

⁷Department of Pediatric Rheumatology, University Hospital Leuven, Leuven, Belgium

⁸Pediatric Unit, "Monsignor Dimiccoli" Hospital, Barletta, Italy

⁹Department of Pediatrics, Faculty of Medicine, Nursing and Health Sciences, Monash University, Clayton, Australia

¹⁰Department of Pediatric Endocrinology and Diabetes, Monash Children's Hospital, Monash Health, Clayton, Australia

¹¹Kariminejad-Najmabadi Pathology and Genetics Center, Tehran, Iran

¹²Department of Metabolic Medicine and Rheumatology, Perth Children's Hospital, Perth, Australia

¹³Western Australian Register of Developmental Anomalies, King Edward Memorial Hospital, Subiaco, Australia

¹⁴Genetic Services of Western Australia, King Edward Memorial Hospital, Perth, Australia

¹⁵Telethon Kids Institute and Division of Pediatrics, School of Health and Medical Sciences, University of Western Australia, Perth, Australia

¹⁶Faculty of Medicine, Notre Dame University, Fremantle, Australia

¹⁷Genetica Medica, Università Campus Bio-Medico, Rome, Italy

¹⁸Medical Genetics Unit, "Antonio Cardarelli" Hospital, Naples, Italy

¹⁹Department of Pediatrics and Adolescent Medicine, American University of Beirut Medical Center, Beirut, Lebanon

²⁰Bone Marrow Transplantation Department, Great Ormond Street Hospital for Children, London, UK

²¹Department of Pediatric Endocrinology and Diabetes, Bristol Royal Hospital for Children, University Hospitals Bristol and Weston NHS Foundation Trust, Bristol, UK

²²Bristol Medical School, Translational Health Sciences, Bristol Medical School, University of Bristol, Bristol, UK

²³San Raffaele Telethon Institute for Gene Therapy SR-Tiget, IRCCS San Raffaele Scientific Institute, Milan, Italy

ABSTRACT

CLC-7 is a chloride-proton antiporter of the *CLC* protein family. In complex with its accessory protein *Ostm-1*, *CLC-7* localizes to lysosomes and to the osteoclasts' ruffled border, where it plays a critical role in acidifying the resorption lacuna during bone resorption. Gene inactivation in mice causes severe osteopetrosis, neurodegeneration, and lysosomal storage disease. Mutations in the human *CLCN7* gene are associated with diverse forms of osteopetrosis. The functional evaluation of *CLC-7* variants might be informative with respect to their pathogenicity, but the cellular localization of the protein hampers this analysis. Here we investigated the functional effects of 13 *CLCN7* mutations identified in 13 new patients with severe or mild osteopetrosis and a known *ADO2* mutation. We mapped the mutated amino acid residues in the homology model of *CLC-7* protein, assessed the lysosomal colocalization of *CLC-7*

Received in original form June 15, 2020; revised form October 21, 2020; accepted October 22, 2020; Accepted manuscript online October 20, 2020.

Address correspondence to: Alessandra Picollo, PhD, Consiglio Nazionale delle Ricerche, Istituto di Biofisica (CNR-IBF), Dulbecco Telethon Laboratory, Genoa, Italy, Via de Marini 6, 16149, Genoa, Italy. E-mail: alessandra.picollo@ge.ibf.cnr.it; Cristina Sobacchi, PhD, Consiglio Nazionale delle Ricerche, Istituto di Ricerca Genetica e Biomedica (CNR-IRGB), Milan Unit, via Fantoli 16/15, 20138, Milan, Italy. E-mail: cristina.sobacchi@humanitasresearch.it

Additional Supporting Information may be found in the online version of this article.

[†]Current address: Department of Anesthesiology, Weill Cornell Medical College, New York, NY USA.

[‡]Current address: Institute of Biosciences and BioResources, Division of Florence, National Research Council (CNR-IBBR), 50019 Sesto Fiorentino, Italy.

Journal of Bone and Mineral Research, Vol. 00, No. 00, Month 2020, pp 1–15.

DOI: 10.1002/jbmr.4200

© 2020 American Society for Bone and Mineral Research (ASBMR)

mutants and *Ostm1* through confocal microscopy, and performed patch-clamp recordings on plasma-membrane-targeted mutant CIC-7. Finally, we analyzed these results together with the patients' clinical features and suggested a correlation between the lack of CIC-7/*Ostm1* in lysosomes and severe neurodegeneration. © 2020 American Society for Bone and Mineral Research (ASBMR).

KEY WORDS: CHLORIDE-PROTON EXCHANGER; LYSOSOMAL LOCALIZATION; MISSENSE MUTATIONS; OSTEOCLAST; OSTEOPETROSIS

Introduction

Bone homeostasis is a complex mechanism that relies on the interplay between osteoblast and osteoclast cells: The former is responsible for bone production, whereas the latter is responsible for bone resorption. Bone degradation requires the acidification of the resorption lacuna, the space created between the bone matrix and the ruffled border membranes of osteoclasts.⁽¹⁾ Key players in the acidification process are the vacuolar-type V-ATPase that drives H⁺ into the resorption lacuna⁽²⁾ and the CIC-7/*Ostm1* protein complex that facilitates acidification⁽³⁾ (Fig. 1A). The CIC-7 protein is an electrogenic chloride/proton exchanger swapping two chloride ions for one proton.⁽⁴⁾ Its interaction with the accessory protein *Ostm1* is required for protein stability and proper function.⁽⁵⁾ Two sources of evidence highlight the role of CIC-7 in osteoclast bone resorption. First, CIC-7 knockout mice develop severe osteopetrosis, a genetic disorder with extremely dense and fragile bones.⁽⁶⁾ In addition, genetic defects in the *CLCN7* gene coding for the CIC-7 protein are present in patients affected by osteopetrosis, which can display different degrees of severity, ranging from lethal to asymptomatic.^(7,8) In particular, CIC-7 missense mutations have been found in patients affected by autosomal recessive osteopetrosis (ARO), the most severe form of which is sometimes associated with primary neurodegeneration (referred to subsequently as “neurodegeneration”), or by autosomal dominant osteopetrosis type II (ADO2). The only available cure for human ARO is hematopoietic stem cell transplantation (HSCT), which, however, is not indicated in patients with neurodegeneration, representing about 50% of CIC-7 ARO cases;^(9,10) consequently, an early diagnosis is critical for defining clinical management.^(11,12) On the other hand, ADO2 may be underdiagnosed, since up to 30% of individuals carrying a *CLCN7* dominant mutation may display neither the classic skeletal phenotype nor other defects.⁽¹³⁾ In symptomatic patients, the onset of the clinical symptoms is usually in late childhood or in adulthood, but severe cases diagnosed in infancy have been described.^(8,14) In ADO2, the mutated allele exerts a dominant negative effect on the dimeric complex, as demonstrated for the p.Gly215Arg mutation, one of the most common in ADO2 patients.⁽¹⁵⁾ In this case, a possible therapeutic strategy under investigation is siRNA-mediated silencing of the mutated allele.⁽¹⁶⁾

Since the first recognition of *CLCN7* mutations in human osteopetrosis, a large number of defects in this gene have been identified. Although the clinical significance of nonsense mutations and insertions/deletions is rather intuitive, classifying missense mutations remains challenging. Missense variants constitute about 60% of the total number of variants in this highly polymorphic gene, based on the number of polymorphisms annotated in common databases. Moreover, mutations are most often found in single families (particularly in relation to recessive cases), therefore comparing the phenotype of affected individuals with the same genotype is generally not

possible; hence, a functional evaluation of the variants is important for assessing possible pathogenicity. In particular, CIC-7 genetic defects could result in absence of the protein, subcellular protein mislocalization, uncoupling of Cl⁻/H⁺ transport, reduced ion transport activity, or accelerated kinetics of transport.⁽³⁾ However, the cellular localization of the protein, essentially on lysosomal membranes and on the osteoclasts' ruffled border, hampers a straightforward analysis of these features.⁽⁵⁾

In 2011, in a pivotal study, Leisle and colleagues identified CIC-7 as a slowly voltage-gated 2Cl⁻/1H⁺ exchanger, set up an electrophysiological assay, and tested 14 *CLCN7* mutations reported in osteopetrotic patients.⁽¹⁷⁾ The genetic heterogeneity of this form of osteopetrosis, as well as the need to define genotype-phenotype correlations possibly relevant for early management, has grown since that time. The work described herein extends Leisle's approach.⁽¹⁷⁾ We used a combination of imaging analysis, electrophysiological measurements, and an optical assay to investigate the functional alterations of 13 different CIC-7 protein mutants carrying previously not-tested missense mutations spread throughout the entire gene and identified in patients affected by different forms of osteopetrosis. We also included in this series of mutations the p.Pro249Leu variant that is recurrently identified in ADO2^(18–20) and has been reported also in two ARO siblings at the compound heterozygous state with the p.Ser744Phe mutation.⁽¹⁴⁾ Our results point to structural-functional correlations that might explain the molecular basis of disease severity.

Materials and Methods

Genetic diagnosis

Specimens, including blood and DNA samples, and clinical data were collected from patients and their parents after informed consent. Mutation analysis of the *CLCN7* gene (GenBank AL031600.4) was performed as previously described.⁽¹⁴⁾ This research complies with the World Medical Association Declaration of Helsinki - Ethical Principles for Medical Research Involving Human Subjects and with the standards established by the Independent Ethical Committee of the Humanitas Clinical and Research Centre.

For patient 8, the molecular analysis was conducted at University Hospitals Bristol and Weston NHS Foundation Trust, in accordance with the standards established by the Declaration of Helsinki and by the Institutional Ethical Committee, using the osteopetrosis virtual panel, including the following genes: *ANKH* (NM_054027.4), *CA2* (NM_000067.2), *CLCN7* (NM_001287.4/NM_001287.5), *CTSK* (NM_000396.3), *FAM123B* (NM_152424.3), *FAM20C* (NM_020223.3), *FERMT3* (NM_178443.2), *IKBK* (NM_001099856.2), *LEMD3* (NM_014319.4), *LRP5* (NM_002335.2), *OSTM1* (NM_014028.3), *SNX10* (NM_001199835.1), *SOST* (NM_025237.2), *TCIRG1* (NM_006019.3), *TGFB1* (NM_000660.4), *PLEKHM1* (NM_014798.2), *PTHR1* (NM_000316.2), *RASGRP2* (NM_001098670.1), *TNFRSF11A* (*RANK*) (NM_003839.2/NM_003839.3),

TNFSF11 (*RANKL*) (NM_003701.3), and *TYROBP* (NM_003332.3). Target sequence enrichment was performed using the Agilent (Santa Clara, CA, USA) Focused Exome Target Enrichment Kit (SureSelectXT) and sequencing was performed using an Illumina (San Diego, CA, USA) NextSeq500 platform. Sequence analysis was carried out exploiting an open-source in-house pipeline, including the BWA-MEM software for alignment to the reference genome (hg19 human genome), GATK HaplotypeCaller (Broad Institute, Cambridge, MA, USA) for genotyping, the Geneticist Assistant tool (SoftGenetics, LLC, State College, PA, USA) for variant annotation and filtering, and the Comprehensive R Archive Network (CRAN) ExomeDepth Package⁽²¹⁾ for the detection of copy number variants. The identified variants were then confirmed using Sanger Sequencing.

Molecular biology and heterologous system

All cDNA used for cell transfection were cloned in the pFrog vector,⁽²²⁾ a modified version of pcDNA3.1 vector suitable for transient transfection in HEK293 cells.

For patch clamp experiments and fluorescence assays, we used the construct characterized by Zanardi and colleagues, in which the C-terminal of Ostm1 is linked through a 2AP cleavage peptide with the N terminal of plasma membrane mutants of rat CIC-7 (CIC-7^{PM}).⁽²³⁾ In turn, the C terminal of CIC-7^{PM} is covalently linked with the E²GFP/DsRed/pH/chloride sensor⁽²⁴⁾ to form the full-construct Ostm1-2AP-CIC-7^{PM}-E²GFP/DsRed-pFrog. HEK293 cells were transfected with 200 to 400 ng of the plasmid. For optical assays, HEK293 cells were cotransfected with this construct and with 200 ng of the Phe-Met-Arg-Phe-NH₂ (FMRFamide)-gated sodium channel PRC_FaNaCh. For the colocalization experiments, HEK293 cells were cotransfected with rCIC-7-eGFP and Ostm1-mCherry. All transfections were performed using the Effectene reagent (Qiagen, Valencia, CA, USA), according to the manufacturer's instructions.

The *CLCN7* mutations were introduced in the wild-type sequence by means of recombinant PCR, using the Fast Mutagenesis System (TransGen Biotech Co, Beijing, China), and confirmed by DNA sequencing.

Electrophysiology

Patch clamp experiments were performed in whole-cell configuration 36 to 48 hours after transfection. Pipettes were pulled from borosilicate glass capillaries (Hilgenberg GmbH, Malsfeld, Germany) and had a resistance of 2 to 3 M Ω in recording solutions. The extracellular solution contained (in mM) 140 NaCl, 2 MgSO₄, 2 CaCl₂, 10 Hepes, pH 7.3. The intracellular solution contained (in mM) 130 CsCl, 2 EGTA, 2 MgSO₄, and 10 Hepes at pH 7.3. Pulses were elicited from a holding potential of 0 mV for 25 ms, followed by voltage steps from -100 to 100 mV with 20 mV increments for 2 seconds (500 ms in the case of the faster mutant p.Leu323Pro) and followed by tail pulse at -60 mV for 500 ms (50 ms for p.Leu323Pro) and back to 0 mV. Data were acquired at 50 kHz after filtering at 10 kHz with an eight-pole Bessel filter using an Axopatch 200 amplifier (Molecular Devices, LLC, San Jose, CA, USA).

To investigate the kinetics of deactivation, we used the following voltage protocol starting from a holding potential of 0 mV for 100 ms: pre-pulse at +80 mV for 1500 ms, followed by voltage steps from -100 to 100 mV with 20 mV increments for 500 ms, then -30 mV pulse for 250 ms.

All data were acquired at room temperature with the custom acquisition program GePulse and analyzed with the custom program Ana (both available at: <http://users.ge.ibf.cnr.it/pusch/>) and SigmaPlot (Systat Software, Inc, San Jose, CA, USA).

Confocal fluorescence microscopy

Transiently transfected HEK293 cells were seeded in glass-bottom petri dishes (purchased from IBL Baustoff + Labor GmbH, Vienna, Austria). Live-cell imaging was performed using a Leica (Buffalo Grove, IL, USA) TCS-SL confocal laser scanning microscope equipped with 63 \times oil immersion objectives (numerical aperture 1.45). Final images are the average of 4 to 12 acquisitions. No filtering was applied. Lysosomes were stained using LysoTracker Deep Red (Thermo Fischer Scientific, Waltham, MA, USA), at a final concentration of 25 nM, 1 hour before visualization. The plasma membrane marker FM4-64 (Thermo Fisher Scientific) was added at a final concentration of 10 μ M in cold solution and cells were immediately recorded.

ImageJ analysis software was used to calculate Mander's colocalization coefficients (MCC).⁽²⁵⁾ To determine the lysosomal trafficking efficiency of CIC-7, Mander's colocalization coefficients between the expression of CIC-7 and lysosomal marker in the full cell were measured. Lysosomal region of interests (ROIs) were used to determine CIC-7/Ostm1 colocalization.

Fluorescence proton assay

Fluorescence proton transport assay was performed following the protocol described by Zanardi and colleagues,⁽⁴²⁾ and Scheel and colleagues.⁽⁴⁵⁾ Briefly, a basic iMIC microscope with a QImaging Retiga EXI Blue camera and a dual-view port for the emission allowing the separation of the GFP and DsRed emissions (Till Photonics GmbH, Kaufbeuren, Germany) were used. For excitation, we used Till Oligochrome (Till Photonics GmbH), a wavelength-switching device containing a stable Xenon light source. Membrane depolarization is necessary to stimulate proton efflux through the CIC-7/Ostm1 complex. We achieved this condition by cotransfecting the epithelial sodium channel FaNaCh, which activates when 30 μ M of FMRFamide is added to the extracellular solution containing (in mM) 138 NaCl, 2 KCl, 10 Hepes, 10 Glucose, 3 MgSO₄, 1.8 CaCl₂, 100 Mannitol, at pH 7.3. The transfected cells were treated with FMRFamide, while excited at 458 nm (100 ms exposition time) and at 482 nm (300 ms exposition time).

For the analysis, we defined $r_{pH} = F_{482} \cdot 3.33 / F_{458}$ measured where signal reaches steady state level. The factor 3.33 stems from the 3.33-fold shorter exposition at the (brighter) excitation wavelength of 482 nm. Data analysis was performed with the custom analysis programs Anavision and Ana (freely available at <http://users.ge.ibf.cnr.it/pusch/>). A region of interest was drawn on the border of the analyzed cell and another on the background for background subtraction.

Data analysis

All data were analyzed with SigmaPlot (Systat Software, Inc). Results were presented as means \pm SD in the tables and as box plots with actual data points, median, mean, and range in the figures. Statistical analysis was performed using unpaired Student's t test with *p* values indicated in the legends. Any *p* values <0.05 were considered statistically significant. The number of independent experiments is indicated by *n*.

Homology model

Phyre2 online software was used to build the human CLC-7 homology model, and Pymol software (Schrödinger Inc., Portland, OR, USA) for protein visualization. The atomic coordinates of the CmCLC three-dimensional structure (3ORG code) served as a template.

Results

Patients' data

In our cohort of unpublished patients with osteopetrosis, we selected 13 affected individuals from 12 unrelated families of various geographic origins, carrying mutations in the *CLCN7* gene not previously subjected to functional assays; moreover, to the best of our knowledge, 12 of the 13 mutations that we evaluated here were novel. Clinical information is reported in a concise form in Table 1, together with genetic data and in an extended form as Supplemental Materials and Methods. Based on the results of the clinical and molecular investigation, 11 of the 13 selected patients were classified as *CLCN7*-deficient ARO because they carried putative biallelic *CLCN7* variants (patients [pt] 1 to 10; pt 2a and pt 2b were affected siblings). Two patients bore a single mutated allele and were classified as ADO2 (pt 11 and pt 12). The patients' age at the onset of the disease ranged from birth (pt 4 and pt 7) to 10 years (pt 8) (median age at onset 3 months) in recessive forms, whereas in the two dominant cases, diagnosis was made in middle childhood (pt 11) or in adolescence (pt 12). Hematological defects (namely, anemia and hepatosplenomegaly) were present in all patients except in pt 8 (recessive) and pt 12 (dominant), whereas pt 6 was anemic owing to alpha thalassemia trait. Six patients, including one ADO2 subject, did not suffer bone fractures, while the others had at least one fracture at different age (details are provided in Supplemental Materials and Methods); remarkably, pt 6 had four fractures. Visual defects of varying severity and likely different origin were present in 9 of 11 recessive cases. Six of these 9 ARO patients displayed signs of progressive neurodegeneration, such as optic nerve atrophy, brain atrophy, epilepsy, hypotonia, and loss of previously acquired skills. On the other hand, pt 12 (dominant) showed a mild reduction of visual capacity but no neurodegeneration. Despite the known high CIC-7/Ostm1 complex expression in the kidney and the importance of endocytosis and lysosomal systems for renal function,⁽³⁾ no signs of altered renal function were reported in any of the enrolled patients; however, we cannot exclude the presence of minor deficits, in accordance with evidence in the *Clcn7*^{G213R} mouse model.⁽²⁶⁾ HSCT was performed only in 2 ARO cases (pt 1 and pt 2b), leading to complete cure in pt 1, while not affecting neurological deterioration in pt 2b, who was in poor condition at 4 years of age with severe cognitive impairment and developmental delay. Among the nontransplanted ARO patients, 5 died in early life owing to bone marrow failure and chronic infection; 3 reached adolescence in reasonably good health, and 2 were lost to follow-up (Table 1).

Regarding genetic data, 7 of 11 ARO cases carried *CLCN7* missense mutations in the homozygous state, while 4 were compound heterozygotes; in particular, pt 4 and pt 6 carried a different missense mutation on each *CLCN7* allele, and pt 1 and pt 9 bore a splicing defect and a missense mutation each. Of note, the p.Ala299Val mutation identified in pt 3 in the homozygous state has been detected also in two Chinese patients,

namely a compound heterozygous ARO affected individual showing also severe neurological impairment and an ADO2 affected individual.^(27,28) To the best of our knowledge, all the other mutations studied herein were novel.

Structural localization

CLC proteins are homodimers and each monomer contains an ion permeation pathway. The transmembrane region is quite large, with 18 alpha helices per monomer (from helix B to helix R), completely or partially spanning the cellular membrane. The cytoplasmic region is composed of two cystathionine β -synthase (CBS) domains, each containing a putative nucleotide-binding site (Fig. 1B, C). In the chloride permeation pathway, a highly conserved glutamate called the external glutamate (Glu_{ext}) constitutes the external gate. When Glu_{ext} is deprotonated, its side chain occupies and closes the chloride pathway; when it is protonated, the side chain moves up and chloride ions can pass through.⁽²⁹⁾ The overall architecture of CLC proteins and the key residues that form the permeation ion pathway are conserved, as demonstrated by the three-dimensional (3D) structure of CLC proteins solved until now^(30–34) and by several experimental data.^(35–38) Consequently, we mapped the selected missense mutations on a 3D homology model of human CIC-7 (hCIC-7) built using the 3D structure of the eukaryotic alga homologue CmCIC as a template.⁽³¹⁾ The very recently solved structures of hCIC-7 in complex with Ostm1 validate our homology model.^(39,40)

The amino acid residues mutated in our series of patients localized to different regions of the protein (Fig. 1B, Supplemental Table S1). Among those affected in cases with ARO and neurodegeneration (pt 2a, pt 2b, pt 3, pt 4, pt 7, pt 9), Arg126 is at the beginning of the first alpha helix B; Ala299 is in the inner part of the protein close to the permeation pathway; Pro582 at the beginning of helix Q, facing the lysosomal lumen; and Gly780 in the cytoplasmic region, in the beta sheet of the CBS2 domain, close to the ATP putative binding site (all shown in red in Fig. 1B, C). Amino acid residues mutated in the remaining 5 patients with ARO with no signs of neurodegeneration (pt 1, pt 5, pt 6, pt 8, pt 10) are exposed at the luminal or cytosol side (Pro376 and Arg791, respectively) and in the transmembrane region of the protein; namely, Ala511 in the loop between helices M-N facing Pro249 in helix F, and Ala590 in the middle of helix Q (all shown in yellow in Fig. 1B, C). The residues mutated in the two ADO2 patients of this series (pt 11 and pt 12) are confined at the interface of the two monomers, close to the cytosolic side (Leu323, at the beginning of helix I), or in the CBS2 domain exposed to the cytoplasm (Lys691) (in blue in Fig. 1B, C). The Pro249 residue is located at the beginning of helix F, just after the external glutamate, in front of Ala511. Finally, the amino acid residue Leu90 is not indicated in the 3D model because it is in a region of CIC-7 N-terminus that is not resolved in the CmCIC structure.

Intracellular localization of CIC-7/Ostm1 protein complexes

The CIC-7/Ostm1 protein complex localizes in the lysosomal membranes, and through exocytosis, it is inserted in the osteoclast ruffled border membrane (Fig. 1A). To assess the subcellular localization of CIC-7/Ostm1 mutants, we produced a series of constructs by introducing each mutation in the rat CIC-7-mCherry (rCIC-7-mCherry) tagged plasmid. In fact, rCIC-7 shows 98% identity with hCIC-7 and well replicates its

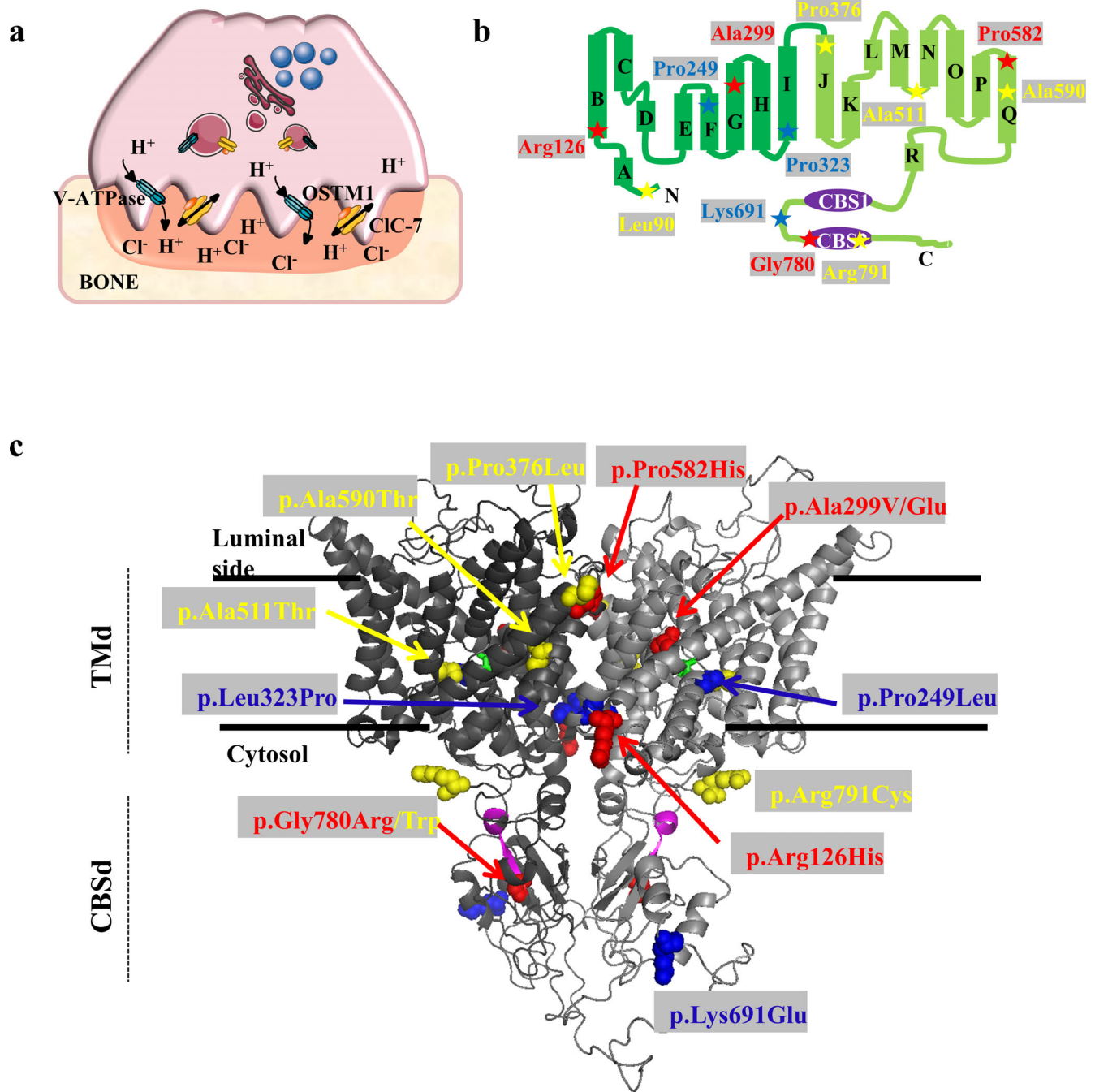


Fig 1. Schematic representation of osteoclast acidification and structural model of human CLC-7. (A) CLC-7 is inserted through lysosomal exocytosis in the convolute plasma membrane of the osteoclasts called ruffled border. The region between the ruffled border and the bone matrix forms the resorption lacuna, the space deputy to bone resorption. The resorption lacuna is acidified by the work of the vacuolar proton pump V-ATPase (in blue) and the CLC-7 exchanger (in yellow). The CLC-7 accessory subunit Ostm1 is shown in orange. (B) Position of analyzed recessive and dominant osteopetrosis causing mutations mapped on the putative topology of the monomer of CLC-7. Mutations found in patients with autosomal recessive osteopetrosis (ARO) and neurodegeneration in this series are shown in red, mutations found in patients with ARO with no neurodegeneration are in yellow, and mutations found in patients with ADO2 are in blue. (C) Mapping of the investigated mutants on the homology model of the human CLC-7 protein based on the structure of the CmCLC homodimer (Protein Data Bank: 3ORG). The two subunits, viewed within the membrane, are colored in gray and light gray. The transmembrane region is indicated as TMD and the cytoplasmic region is indicated as CBSd. Mutated residues in both subunits are shown as spheres. Mutations are colored as in B. The green stick in each subunit corresponds to the external glutamate. The ATP putative binding sites are colored in magenta.

Table 1. Main Clinical Findings in the Novel CLCN7-Deficient Osteopetrotic Patients

| Pt no. | Genetics | Geographic origin | Age at onset | Hematological defects | Bone fractures | Neurological defects | | | Outcome | |
|--------|--|------------------------|-------------------|--|-----------------------------------|----------------------|------------------|---------------|---------------------------|--|
| | | | | | | Vision | Hearing | PN HSCT (age) | | |
| Pt 1 | c.[269 T > C]; [982-1G > T] p.Leu90Pro; r.spl? | European (non-Finnish) | 3 mo | Anemia, hepatosplenomegaly | None | Blind | Normal | No | Yes (6 mo; 7,5 mo; 15 mo) | Alive and well at 20 yr |
| Pt 2a | c.[377G > A]; [377G > A] p.Arg126His; Arg126His | Egyptian Arabic | 3 mo | Pancytopenia, hepatosplenomegaly | Yes (2 at 12 mo) | Blind | Deaf | Yes | ND | Died at 19 mo (BM failure) |
| Pt 2b | c.[377G > A]; [377G > A] p.Arg126His; Arg126His | Egyptian Arabic | 2 mo ^a | Hepatosplenomegaly | None | Reduced | Normal | Yes | Yes (5 mo) | Severe psychomotor delay and cognitive impairment at 4 yr |
| Pt 3 | c.[896C > T]; [896C > T] p.Ala299Val; Ala299Val | Iranian | 2 mo | Anemia, hepatosplenomegaly | None | Severely reduced | Severely reduced | Yes | ND | Died at 5 mo (chronic osteomyelitis) |
| Pt 4 | c.[718G > A]; [896C > A] p.Gly240Arg; Ala299Glu | European (non-Finnish) | At birth | Anemia, hepatosplenomegaly, thrombocytopenia | Yes | Severely reduced | Severely reduced | Yes | ND | Died at 15 mo (pneumonia) |
| Pt 5 | c.[1127C > T]; [1127C > T] p.Pro376Leu; Pro376Leu | Moroccan | 7 mo | Anemia, splenomegaly | Yes (1 at 59 mo; 1 at 75 mo) | Severely reduced | Severely reduced | No | ND | Delayed psychomotor development and cognitive impairment at 8 yr |
| Pt 6 | c.[1531G > A]; [2338G > T] p.Ala511Thr; Gly780Trp | European (non-Finnish) | 5 yr | Anemia ^b | Yes (1 at 5 yr; 3 more, later on) | Normal ^c | Normal | No | ND | Alive and well at 16 yr |
| Pt 7 | c.[1745C > A]; [1745C > A] p.Pro582His; Pro582His | Iraqi | At birth | Pancytopenia, hepatosplenomegaly | None | Cone-rod dystrophy | No | Yes | ND | Died at 21 mo |
| Pt 8 | c.[1768G > A]; [1768G > A] p.Ala590Thr; Ala590Thr | Romanian | 10 yr | None | Yes (1 at 10 yr) | Normal | Normal | No | ND | Alive and well at 12 yr |
| Pt 9 | c.[676-10,11 del]; [2338G > A] r.spl?; p.Gly780Arg | European (non-Finnish) | 5 wk | Pancytopenia | None | Blind | Normal | Yes | ND | Died at 35 mo (BM failure) |
| Pt 10 | c.[2371C > T]; [2371C > T] p.Arg791Cys; Arg791Cys | Lebanese | 9 yr | Anemia, hepatosplenomegaly | Yes (1 at 7 yr) | Severely reduced | No | No | ND | Lost at follow-up |
| Pt 11 | c.968 T > C; [=] p.Leu323Pro; [=] | Turkish | 8 yr | Mild anemia | Yes (1 at 8 yr) | No | No | No | ND | Lost at follow-up |
| Pt 12 | c.2071A > G; [=] p.Lys691Glu; [=] | European (non-Finnish) | 5.5 yr | None | None | Mildly reduced | No | No | ND | Alive and well at 20 yr; chronic bone pain |

Pt no. = patient number; PN = progressive neurodegeneration, as defined in ref. 59; HSCT = hematopoietic stem cell transplantation; mo = months; yr = years; ND = not done; BM = bone marrow; wk = weeks. Accession number of the CLCN7 cDNA: AF224741; the numbering used starts with nucleotide +1 for the A of the ATG-translation initiation codon. Red color indicates the mutations functionally evaluated in the framework of the present work.

^aPrenatal diagnosis was performed in this patient.

^bAnemia in this patient was secondary to alpha thalassemia trait.

^cCongenital anomalous optic nerves.

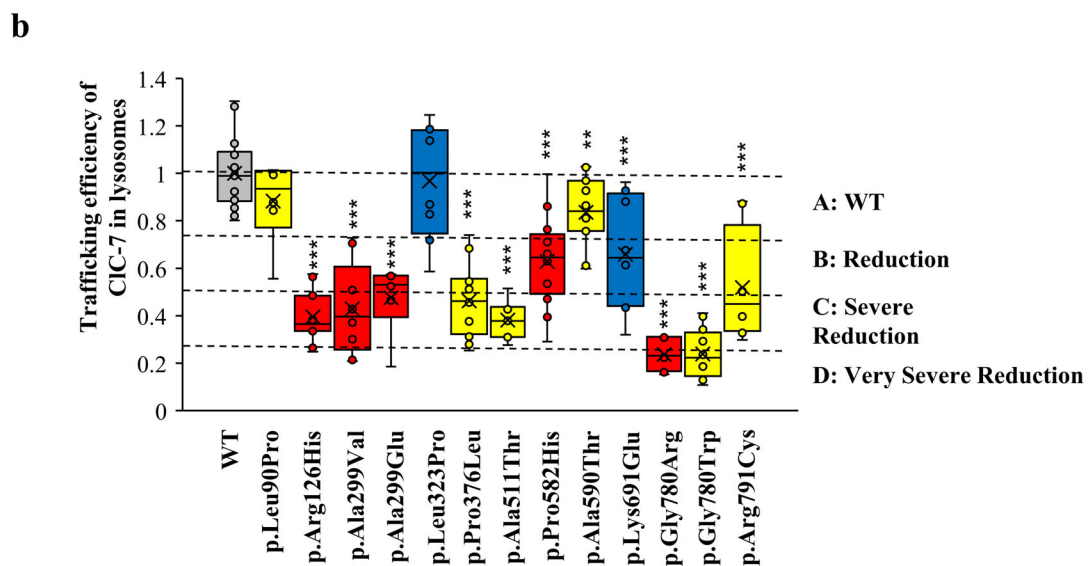
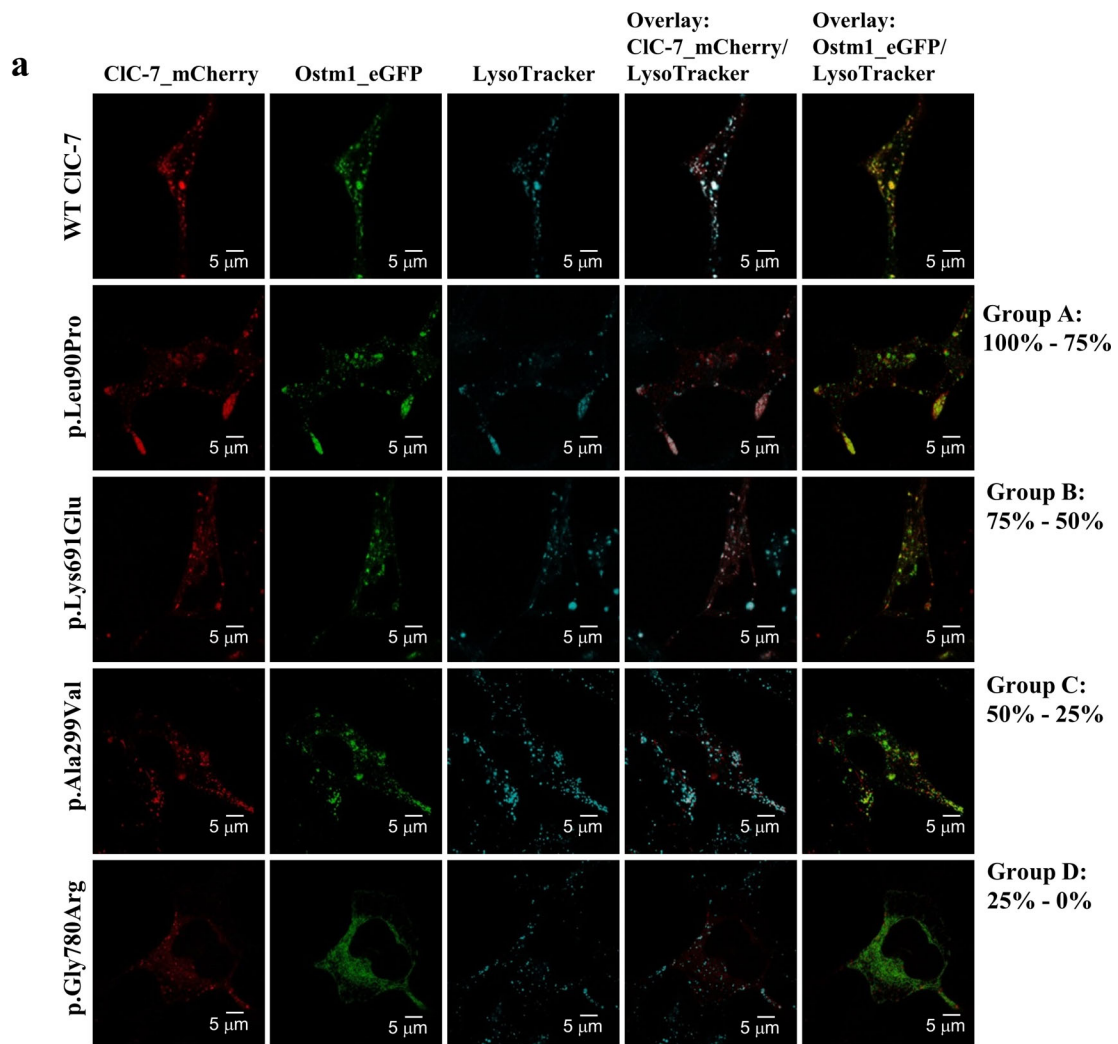


Fig 2. Legend on next page.

electrophysiological properties.⁽¹⁷⁾ Nonetheless, to avoid confusion between genetic and functional data, in this article, we refer to the mutants using the human protein terminology.

Each rCIC-7-mCherry plasmid was cotransfected with the Ostm1-eGFP labeled construct into HEK293 cells. The two fluorescent proteins allowed us to simultaneously determine by confocal analysis whether CIC-7 is expressed into the lysosomes (in turn stained with a specific chemical marker) and whether CIC-7 and Ostm1 colocalized (Fig. 2, Supplemental Fig. S1.). Using Mander's colocalization coefficient (MCC; see Materials and Methods), we measured trafficking efficiency of WT and mutant CIC-7 proteins to the lysosomes and the relative colocalization of CIC-7 and Ostm1 at the lysosomes.

Wild-type (WT) CIC-7 colocalized very well with lysosomes (MCC = 0.70), indicating preserved protein trafficking despite overexpression. MCC of CIC-7 mutants was normalized to WT, and based on the results, the mutants were divided into four groups (from A [moderate effect] to D [very severe effect]), with a 25% reduction in the efficiency of lysosomal trafficking with each passage from the previous to the next (Fig. 2B, Table 2). Group A ($\geq 75\%$ of localization to lysosomes compared with WT) comprised three mutants (p.Leu90Pro, found in pt 1, p.Leu323Pro in pt 11, and p.Ala590Thr in pt 8); group B (50% to 75% of localization to lysosomes compared with WT) three mutants (p.Pro582His, found in pt 7, p.Lys691Glu in pt 12, and p.Arg791Cys in pt 10); group C (25% to 50% of localization to lysosomes compared with WT) five mutants (p.Arg126His, found in pt 2a and pt 2b, p.Ala299Val in pt 3, and p.Ala299Glu in pt 4, p.Pro376Leu in pt 5, and p.Ala511Thr in pt 6). Finally, in group D (<25%), we observed an almost complete delocalization of the two mutants (p.Gly780Arg and p.Gly780Trp, found in pt 9 and pt 6, respectively), indicating that these mutations drastically impaired CIC-7 trafficking. However, we cannot exclude an altered protein folding, owing to the marked difference of the physicochemical properties of the amino acid residues involved. On the other hand, for all mutants, we observed that CIC-7 distribution closely resembled that of Ostm1, with a relative percentage of colocalization in lysosomes between 60% and 100% compared with WT (Supplemental Table S2). This last result suggests that the pathogenic effects are not due to the disruption of the interaction between CIC-7 and Ostm1 for any mutation. Based on these data, we observed that overall patients bearing mutations belonging to groups A and B developed less severe disease (the ARO patients pt 1, pt 8, pt 10 and the two ADO patients pt 11 and pt 12), whereas patients bearing mutations that significantly impaired protein localization (groups C and D) showed a more severe phenotype including also primary neurodegeneration (pt 2a and pt 2b, pt 3, pt 4, and pt 9). Interestingly, for the p.Pro249Leu mutant, we were not able to determine either the lysosomal localization or the colocalization with Ostm1 because in all repeated experiments,

the transfected cells were adversely affected and died the day after transfection.

Alteration of chloride transport by CIC-7 mutants

Among the 13 selected mutations, 11 showed a preserved or only partially reduced lysosomal localization, suggesting that the affected function was mainly ion transport rather than protein trafficking or folding instability. To investigate the functional properties of these mutants, we took advantage of previous studies showing that the disruption of the di-leucine lysosomal sorting motif in the N-terminus of CIC-7 induced a partial relocation of CIC-7 plasma membrane mutants (CIC-7^{PM}) to the plasma membrane, thereby allowing electrophysiological measurements.⁽⁴¹⁾ Therefore, the selected CIC-7 mutations were inserted in the rCIC-7^{PM} background. Moreover, to ensure the simultaneous expression of both Ostm1 and CIC-7, the two proteins were linked by a self-cleavable 2A peptide and, to measure proton and chloride transport, a chloride/pH sensor (E₂GFP/DsRed) was fused with the C-terminus of rCIC-7^{PM}.⁽⁴²⁾ Chloride currents were recorded with the patch clamp technique in HEK293 cells transiently transfected with WT or mutant rCIC-7^{PM}/Ostm1 cDNA. All investigated mutants partially relocate to the plasma membrane (Supplemental Fig. S2). Those featuring p.Ala299Val/Glu, p.Ala511Thr, p.Ala590Thr, p.Pro582His, and p.Gly780Arg/Trp (carried by pt 3 and pt 4, pt 6, pt 8, p7, and pt 9, respectively) did not show significant chloride currents. The remaining mutants (p.Leu90Pro, p.Arg126His, p.Leu323Pro, p.Pro376Leu, p.Lys691Glu, and p.Arg791Cys) found in pt 1, pt2a and b, pt 11, pt 5, pt 12, and pt 10, respectively, showed the same voltage dependence as WT (Fig. 3A, B) with a reduction in the currents' density and/or a decrease in the rate of activation and deactivation of the channel (Fig. 3C). Specifically, the p.Lys691-Glu mutant showed 35% reduction in the density of currents and kinetics similar to WT (Fig. 3C, Table 2). The p.Leu90Pro, p.Leu323Pro, and p.Arg791Cys mutants had density of currents similar to WT but faster kinetics of activation (p.Leu323Pro and p.Arg791Cys) and deactivation (p.Leu90Pro, p.Leu323Pro, and p.Arg791Cys) compared with WT. For the p.Leu323Pro mutant, we observed the largest change in the kinetics of activation compared with WT, with a time constant of activation of 50 ms (versus 490 ms for WT) at +80 mV and kinetics of deactivation almost threefold faster than the WT (Fig. 3C, Table 2). Finally, the p.Arg126His and p.Pro376Leu mutants showed a strong reduction in the total currents, coupled with an alteration of gating kinetics (Fig. 3C, Table 2). Comparing the localization data with these functional results, we noticed that the mutations classified in groups A and B (ie, displaying more than 50% of the normal localization) maintained at least 60% of the chloride and proton transport carried out by the WT channel, supporting a correlation with the milder osteopetrotic phenotype of the corresponding

FIGURE 2 Subcellular localization of the CIC-7 mutations investigated in this work. (A) Representative images of the subcellular localization of CIC-7-mCherry and mutants co-expressed with Ostm1-eGFP. The LysoTracker deep red is colored in cyan. Overlay of rCIC-7-mCherry and the lysosomal marker fluorescence and of rCIC-7-mCherry and Ostm1-eGFP fluorescence is shown in the last two columns, respectively. We selected only one mutant per each group of classification (from A to D). The percentage of lysosomal localization reduction normalized to WT CIC-7 lysosomal localization is indicated on the right of each row. Images for all the other mutants are reported in Supplemental Fig. S1.. (B) Relative expression level of mutants in the lysosomes normalized to the expression level of WT in the lysosomes. Mutants are defined as in Fig. 1 (gray = WT; red = ARO with neurodegeneration; yellow = ARO without neurodegeneration; blue = ADO2). Dashed lines indicate the relative expression level of 100%, 75%, 50%, and 25%. Results are presented as box plots with actual data points, median, mean, and range with $n > 6$ independent experiments. Unpaired Student's *t* test was used for statistical analysis of normalized data of all mutants investigated. Statistical significance is denoted versus WT (control): ** $p < 0.01$; *** $p < 0.001$.

Table 2. Biophysical Parameters of WT CIC-7^{PM} and Mutants at +80 mV

| CIC-7 ^{PM} | SSC (pA/pF) | τ_{act} (ms) activation | τ_{deact} (ms) deactivation | <i>n</i> | Δr_{pH} | <i>n</i> |
|---------------------|-------------------|------------------------------|----------------------------------|----------|--------------------|----------|
| WT | 24.5 ± 8.5 | 487 ± 187 | 27 ± 5 | 13 | 1.04 ± 0.2 | 37 |
| p.Leu90Pro | 21.8 ± 5.3 | 436 ± 190 | 19 ± 8 | 11 | 0.76 ± 0.2 | 49 |
| p.Arg126His | 8.5 ± 4.0 | 277 ± 63 | 10 ± 4 | 8 | 0.54 ± 0.2 | 27 |
| p.Leu323Pro | 29.4 ± 3.7 | 36 ± 17 | 10 ± 4 | 10 | 1.18 ± 0.3 | 21 |
| p.Pro376Leu | 8.1 ± 2.1 | 367 ± 98 | 19 ± 3 | 6 | 0.21 ± 0.08 | 27 |
| p.Lys691Glu | 15.7 ± 2.8 | 605 ± 227 | 26 ± 8 | 11 | 0.8 ± 0.1 | 23 |
| p.Arg791Cys | 23.2 ± 5.2 | 273 ± 90 | 17 ± 5 | 12 | 0.97 ± 0.2 | 37 |

SSC = steady-state currents expressed as currents density; τ_{act} and τ_{de-act} = time constants of activation and deactivation, respectively; Δr_{pH} = mean values of changes of r_{pH} ; *n* = number of experiments; WT = wild type.

All data are expressed as means ± SD. In bold are the values that are statistically different with *p* < 0.05 or less compared with WT.

patients (pt 1, pt 10, pt 11, and pt 12). For the p.Lys691Glu mutation in pt 12, the overall clinical manifestation could be likely dampened by the expression of the WT allele. On the other hand, mutants classified in groups C and D (ie, p.Ala299Val/Glu, p.Ala511Thr, p.Ala590Thr, p.Pro582His, and p.Gly780Arg/Trp, with a strong reduction in lysosomal localization) displayed an absence or drastic reduction of ion transport, which overall fit well with the more severe phenotype presented by the corresponding patients (pt 2, pt 3, pt 4, pt 9).

Coupling of chloride and proton transport is preserved in CIC-7 mutants

The investigation of two *CLCN7* knock-in mice, namely the uncoupled mouse model *CLCN7^{unc/unc}*, where only chloride conductance was preserved, and the transport-deficient mouse model *CLCN7^{td/td}*, in which the transport of both chloride and proton ions was abolished but the correct protein trafficking was preserved, highlighted the fundamental role of the chloride/proton exchange activity in the physiological functions of CIC-7.^(43,44) Consequently, we determined whether chloride transport was still coupled with proton transport in the presence of the mutants by means of an optical assay, as published.^(42,45) In detail, we monitored the change in the fluorescence signal of the E²GFP/DsRed sensor,⁽²⁴⁾ due to the dequenching by protons that moved out of cytosol mediated by CIC-7 transport activity. In this kind of assay, the fluorescence ratio F482/F458 = r_{pH} directly reflects changes in the intracellular pH. CIC-7 activates at membrane potentials greater than +20 mV, so depolarization of the plasma membrane was necessary to activate CIC-7. We achieved this condition by cotransfecting the construct of interest with the sodium channel FaNaCh, which was activated by the FRMRamide peptide (Fig. 4A).^(42,45) Upon FRMRamide exposure, the sodium channel was activated and depolarized the plasma membrane, thereby in turn activating the rCIC-7/Ostm1 protein complex and causing proton efflux. We tracked proton efflux by measuring the increase in the fluorescence signal. Using this strategy, we tested all mutants and found that only those mutants that had retained the ability to generate ion currents in patch-clamped cells were able to transport protons (Fig. 4A, Table 2). Despite the qualitative nature of the optical assay, there was a strong correlation between the magnitude of chloride and proton transport: Mutants with a strong decrease in ion current density also showed the maximal proton flux reduction (Fig. 4B). Therefore, based on our results, none of the human mutations herein studied replicated the condition described in the *CLCN7^{unc/unc}* mouse model; in fact, mutants that transported chloride ions maintained the coupling

with proton transport. On the other hand, the p.Ala590Thr mutant was the only one among the tested mutants that resembled the *CLCN7^{td/td}* model; in fact, ion transport was absent, while the protein was correctly expressed on the lysosomes.

Discussion

Osteopetrosis caused by *CLCN7* mutations is classified as infantile malignant autosomal recessive osteopetrosis (ARO)⁽⁶⁾ or as autosomal dominant osteopetrosis type II (ADO2 or Albers-Schonberg disease).^(18,46) The heterogeneity of the clinical phenotypes and the large variety of *CLCN7* variants represents a challenge in the identification of genotype-phenotype correlations. Regarding the underlying disease mechanism, the functionality of the CIC-7/Ostm1 protein complex can be altered by defects in the cellular localization and/or in the molecular mechanisms of anion transport.

Here we investigated the functional effects of 14 missense mutations found in the *CLCN7* gene in patients affected by diverse forms of osteopetrosis. Table 3 summarizes our results correlating the physiological and functional data with the clinical phenotype, and the following subsections contextualize our findings in relation to published literature.

Summary of results and conclusions on ADO2 mutations

For the ADO2 in our series (p.Leu323Pro and p.Lys691Glu), we observed normal or partial reduction in the expression level of CIC-7 and Ostm1 in lysosomes. When we forced their expression on the plasma membrane, we recorded chloride and proton fluxes for both CIC-7 mutants; however, the p.Lys691Glu showed a decrease in current intensity, while the p.Leu323Pro mutant had faster kinetics of activation. This latter finding is in agreement with the gating kinetics reported for other mutants associated with ADO2 (p.Leu213Phe, p.Arg286Gln, p.Pro619Leu, p.Arg762Leu, and p.Arg767Gln).⁽¹⁷⁾ A common feature of all these mutants is that they are located at the interface between the transmembrane and the cytosolic region of the protein (Supplemental Fig. S3). We might speculate that in general mutations in this region accelerate gating kinetics, which in turn alters the slow gating that is essential for the simultaneous opening of the two ion pathways through a global protein conformational change.⁽⁴⁷⁾ Interestingly, evidence of the relevance of CIC-7 gating kinetics for proper osteoclast function have also been obtained in other species. Sartelet and colleagues found that severely affected osteopetrotic calves of the Belgian Blue cattle breed were homozygous for the spontaneous p.Tyr750Gln (Tyr746 in hCIC-7) amino acid change in the CIC-7

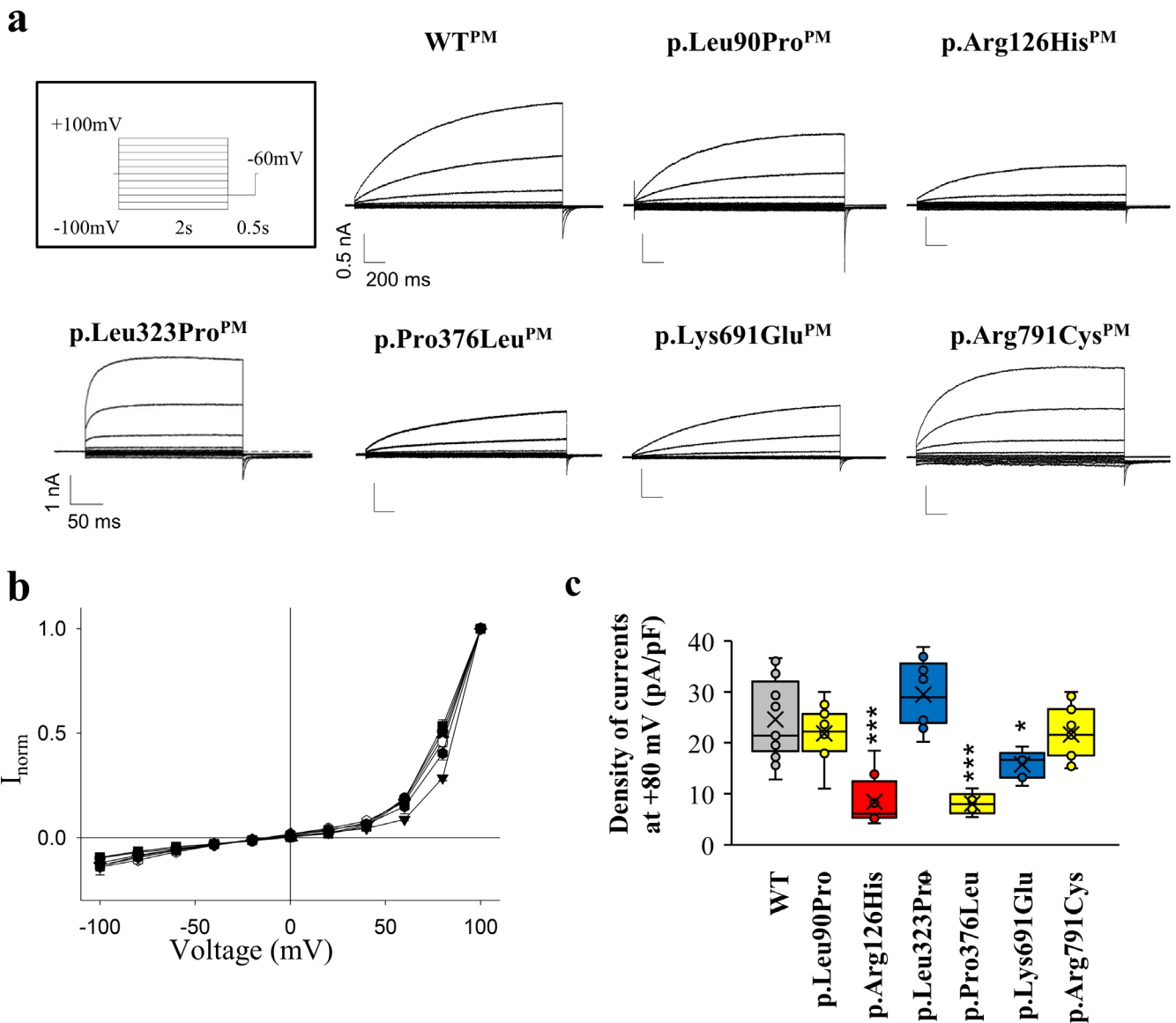


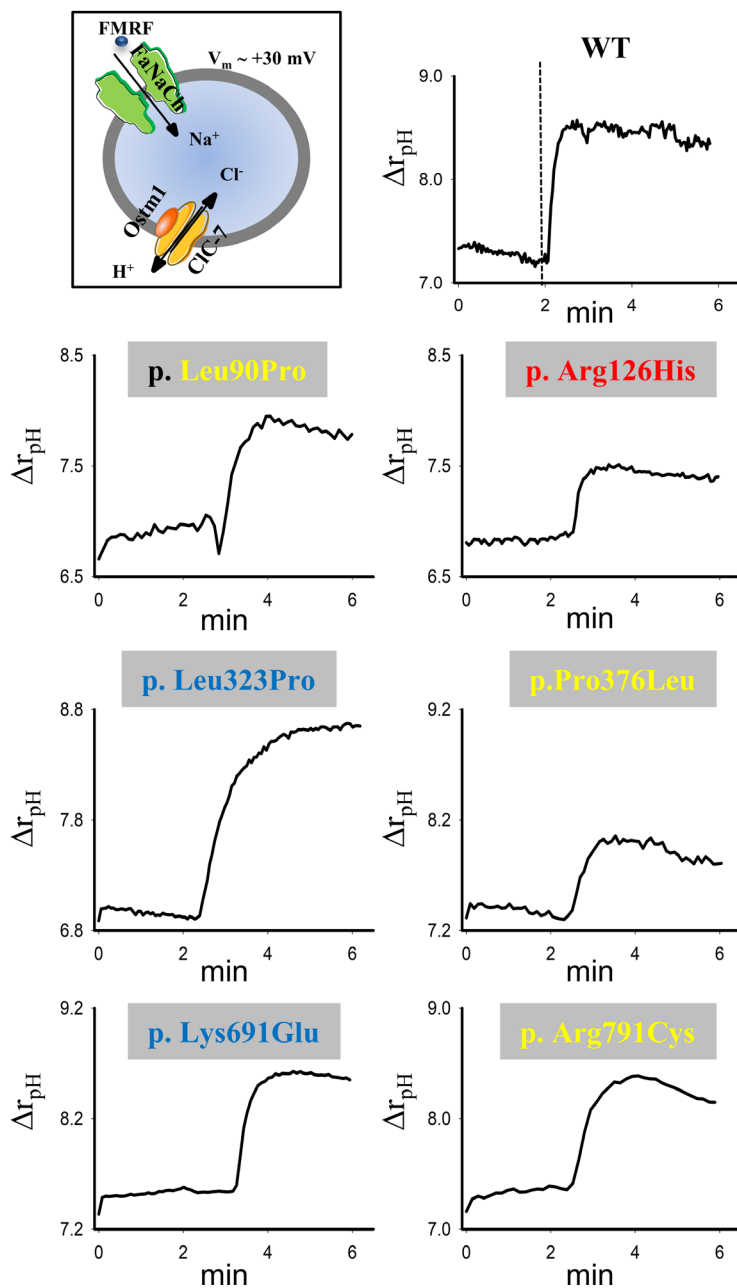
Fig 3. Functional characterization of CIC-7^{PM} and mutants. (A) Representative current traces of WT and mutant CIC^{PM}. Inset: stimulus protocol. Currents were recorded from transfected HEK293 cells. Currents were elicited from a holding potential of 0 mV for 25 ms, followed by voltage steps from -100 mV to 100 mV with 20 mV increments for 2 seconds (for 500 ms in the case of the faster mutant p.Leu321Pro) and followed by tail pulse at -60 mV pulse for 500 ms (50 ms for p.Leu321Pro) and back to 0 mV. Scale bars for each mutant are as in the WT traces, with the exception of p.Leu323Pro. (B) I-V curve for all the mutants. WT = black circle; p.Leu90Pro = black up triangle; p.Arg126His = black down triangle; p.Leu321Pro = black square; p.Pro376Leu = black hexagon; p.Lys691Glu = black diamond; p.Arg791Cys = open square. (C) Box plot of the density of currents measured at +80 mV for WT and all six mutants. Mutants are defined as in Fig. 1 (gray = WT; red = ARO with neurodegeneration; yellow = ARO without neurodegeneration; blue = ADO2). Results were presented as box plots with actual data points, median, mean, and range with $n > 5$ independent experiments. Unpaired Student's t test was used for statistical analysis of all mutants investigated. Statistical significance is denoted versus WT (control): * $p < 0.05$; *** $p < 0.001$.

protein.⁽⁴⁸⁾ The affected residue was in the CBS2 domain, at the interface between the transmembrane region and the two cytosolic subunits (Supplemental Fig. S3), similarly to the above listed “fast mutations.” Accordingly, the p.Tyr750Gln missense mutation significantly accelerated the gating kinetics, while it had little effect on protein localization and expression level. The zygosity status of the mutation in the affected calves might be responsible for the severity of the disease compared with the human mutations above mentioned, which have been

found only at the heterozygous state, to the best of our knowledge.

Recently, Nicoli and colleagues reported a new de novo missense mutation of CIC-7 (p.Tyr715Cys) in two unrelated patients presenting lysosomal storage disease and albinism but without osteopetrosis.⁽⁴⁹⁾ Also, in this case the mutation localized in the CBS2 domain, but apparently it was exposed to the cytosol far from the dimer interface (Supplemental Fig. S3, in cyan). Moreover, the absence of a skeletal

a



b

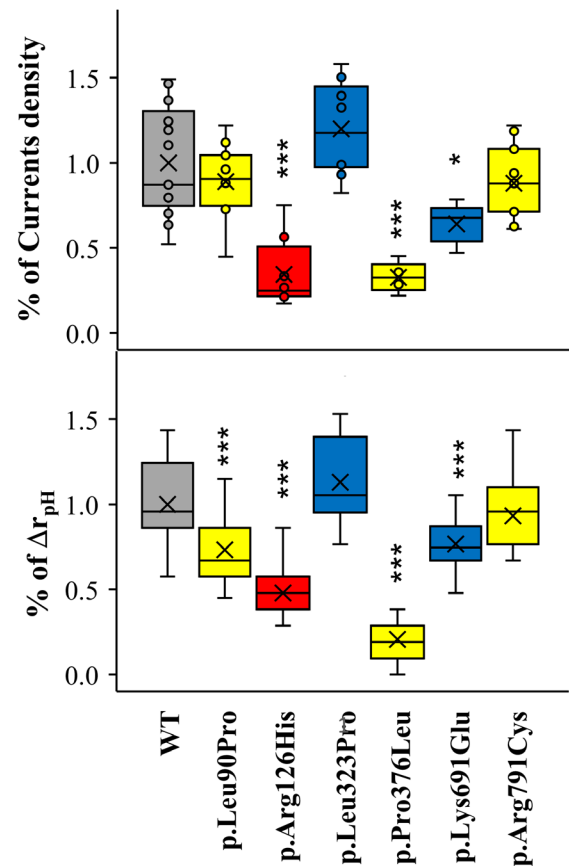


Fig 4. Chloride/proton transport coupling is preserved in the mutants. (A) Representative proton transport traces for WT rCIC-7^{PM} and mutants. The change of $r_{pH} = F_{482} \cdot 3.33 / F_{458}$ (Δr_{pH}) is plotted versus the time. After 2 minutes, the FMRF peptide was added to induce membrane depolarization and thereby CIC-7 activation. Dashed bar in the WT plot indicates the time (2 minutes) corresponding to the addition of FMRF peptide. A schematic representation of the optical assay is shown in the inset. (B) Changes in chloride and proton transport activity. Chloride currents density from Fig. 3B normalized to the WT currents density at +80 mV are shown in the top box plot. Changes in the r_{pH} normalized in respect to the WT value are shown in the bottom box plot. Results were presented as box plots with actual data points, median, mean, and range with $n > 21$ independent experiments. Unpaired Student's t test was used for statistical analysis of normalized data of all mutants investigated. Statistical significance is denoted versus WT (control): *** $p < 0.001$.

phenotype in the patients and the extensive formation of enlarged vacuoles in cells expressing the mutated protein (a feature never observed in cells transfected with our series of mutants) would point to a completely different

pathogenetic mechanism. This further extends the variety of phenotypes caused by defects in the *CLCN7* gene.

The role of the accelerated activation kinetics of CIC-7 in the CIC-7/Ostm1 biological function remains unclear. We might

Table 3. Comparison of Clinical, Physiological, and Functional Data

| Mutant | Clinical diagnosis | Lysosomal trafficking efficiency | Currents density | Gating kinetics | Proton transport |
|--------------------------|--------------------|----------------------------------|------------------|-----------------|------------------|
| p.Arg126His | ARO + Neuro | Severely reduced | Severely reduced | Altered | Severely reduced |
| p.Ala299Val | | Severely reduced | Abolished | NM | Abolished |
| p.Ala299Glu | | Severely reduced | Abolished | NM | Abolished |
| p.Pro582His | | Mildly reduced | Abolished | NM | Abolished |
| p.Gly780Arg | | Very severely reduced | Abolished | NM | Abolished |
| p.Leu90Pro | ARO | Normal | Normal | Altered | Normal |
| p.Pro376Leu | | Severely reduced | Severely reduced | Altered | Severely reduced |
| p.Ala590Thr | | Normal | Abolished | NM | Abolished |
| p.Ala511Thr ^a | ADO2 | Severely reduced | Abolished | NM | Abolished |
| p.Gly780Trp ^a | | Very severely reduced | Abolished | NM | Abolished |
| p.Arg791Cys | | Mildly reduced | Normal | Altered | Reduced |
| p.Pro249Leu | | NM | NM | NM | NM |
| p.Leu323Pro | | Normal | Normal | Altered | Normal |
| p.Lys691Glu | | Mildly reduced | Reduced | Normal | Reduced |

NM = not measurable.

For each mutant herein analyzed, the level of reduction in the efficiency of lysosomal trafficking, the change in the current density, gating kinetics, and proton transport are reported.

^aThe mutations that are present in the compound heterozygous state in pt 6.

propose that, if the voltage dependence of the CIC-7^{PM} is the same as in the native lysosomes, CIC-7 might be insensitive to quick membrane voltage changes, which could be produced after release of calcium or during fusion events. To elucidate the possible role in the lysosomal homeostasis of fast mutants, Astaburuaga and colleagues developed a mathematical model that predicts a differential effect of chloride transport on calcium dynamics: In the presence of faster gating kinetics of CIC-7, Ca²⁺ concentration and peak Ca²⁺ release is weaker.⁽⁵⁰⁾ Lysosomal calcium release regulates lysosomal exocytosis that is necessary for ruffled border formation. Consequently, the pathogenicity of these fast mutants might arise from the altered calcium dynamics; this hypothesis deserves further elucidation.

For what pertains to the p.Pro249Leu mutation, which is common in ADO2, we were not able to perform any kind of measurement because the cells transfected with this construct died shortly after transfection. Such a dramatic effect was unexpected, based on the benign presentation of the disease in the patients.^(18,46) In ADO2, the dimeric nature of CIC-7 protein implies that normal homodimer and mutated homo-heterodimers could be simultaneously present in the cell, with two possible consequences: Either the presence of 25% of WT homodimer is sufficient to mitigate the pathological effect of the mutant or, on the contrary, the single mutation has a dominant negative effect despite the occurrence of 25% of WT homodimer. We might speculate that in ADO2 cases carrying the p.Pro249Leu CIC-7 mutation the residual 25% of WT dimers is sufficient to maintain a sufficient osteoclast activity. To the best of our knowledge, the p.Pro249Leu CIC-7 mutation has never been described in a patient in the homozygous state. In vitro, the severe toxicity of the homozygous p.Pro249Leu mutant could be associated with a strong chloride leak. In fact, the exchange of a proline with a leucine residue could introduce a drastic change in the flexibility of the backbone of helix F that is part of the chloride permeation pathway keeping each single anion pathway in a constitutive open state, thereby causing free chloride diffusion.

Summary of results and conclusions on ARO mutations

Regarding the mutations of the ARO patients herein investigated, our results suggested that different functional properties

were displayed by those found in cases with (pt 2a, pt 2b, pt 3, pt 4, pt 7, pt 9) or without (pt 1, pt 5, pt 6, pt 8, pt 10) signs of primary neurodegeneration. The former group comprised the mutations p.Arg126His, p.Ala299Val/Glu, p.Pro582His, and p.Gly780Arg. All of them showed a partial or severe reduction in the level of lysosomal localization. Moreover, all except p.Arg126His lacked transport activity, when the mutants were forced to reach the plasma membrane, whereas the p.Arg126His mutant showed 33% residual activity. We suggest that the severe trafficking defect causing the absence of CIC-7/Ostm1 complex on the lysosomal membranes, rather than the absence or reduction in the efficiency of chloride/proton exchange, could result in the neurodegenerative phenotype. In agreement with this interpretation, Leisle and colleagues previously reported that the mutations p.Gly240Arg (also carried by pt 4 in our cohort, in the compound heterozygous state), p.Arg526Trp, and p.Gly521Arg, found in ARO patients with neurodegeneration, showed retention in endoplasmic reticulum and no transport activity.⁽¹⁷⁾ The hypothesis that the aberrant localization of the CIC-7/Ostm1 complex might be implicated in the neurodegenerative phenotype is corroborated by the clinical evidence in ARO patients with defects in the *Ostm1* gene (mostly, truncating mutations), which invariably present severe neurodegeneration. In this specific subgroup of patients, the few reported mutations are severely truncating defects likely resulting in the substantial reduction or absence of the Ostm1 protein.⁽¹¹⁾ Even though not formally demonstrated in human samples, the expected consequence based on in vitro studies would be CIC-7 destabilization, lack of proper localization, and function. OSTM1-deficient ARO is recapitulated by the gray lethal (*gl*) mouse model,⁽⁵¹⁾ in which the Ostm1 protein is absent, thus precluding the formation of the CIC-7/Ostm1 protein complex, and CLCN7 protein levels are decreased below 10% of normal;⁽⁵⁾ indeed, *gl* mice manifest severe neurodegeneration.^(52–54) Finally, the homozygous CIC-7^{G213R} knock-in mouse showed osteopetrosis and severe neurodegeneration caused by a severe trafficking defect.⁽⁵⁵⁾

The mutations found in patients without neurodegeneration in our series were p.Leu90Pro, p.Pro376Leu, p.Ala511Thr, p.Gly780Trp/Arg, p.Ala590Thr, and p.Arg791Cys (Table 1). We observed conserved ion transport activity with altered

biophysical properties, specifically, a reduction in the density of the total currents and/or faster kinetics of activation and deactivation (p.Leu90Pro, p.Pro376Leu, and p.Arg791Cys), associated with relative normal lysosomal localization for p.Leu90Pro and p.Arg791Cys mutants. In this group, the p.Pro376Leu mutant showed the most severe alteration, probably because of the reduction of the lysosomal localization associated with a strong reduction in the total chloride currents; accordingly, the clinical picture of the corresponding patient in this series (pt 5) was serious. The p.Leu90Pro mutant was localized in the N terminus of CIC-7, where two dileucine AP-binding motifs are essential for lysosomal targeting of CIC-7.⁽⁴¹⁾ Even though we did not observe significant changes in the lysosomal localization of the p.Leu90Pro mutant, we cannot exclude that it might be part of a lysosomal sorting motif used *in vivo*. The interpretation of the results is less straightforward for pt 6, whose main clinical feature was the occurrence of repeated fractures. The proband was a compound heterozygote for p.Ala511Thr and p.Gly780Trp, which in our *in vitro* assays displayed a severe reduction in the subcellular localization and absence of transport activity. In our experimental set up, a single mutant at a time was overexpressed in HEK293 cells, so it might be hypothesized that the drastic alteration of the functional properties observed for the two single mutants could be attenuated when they are co-expressed and form a heterodimeric complex. Moreover, the p.Gly780Trp was maternally inherited and the patient's mother showed only increased bone density, possibly suggesting that both the mutations were essential for clinical disease manifestation and partially compensated for each other. The biallelic p.Ala590Thr variants carried by pt 8 is challenging to understand at a molecular level: *in vitro* assays showed preserved lysosomal localization and a total absence of transport, while the patient had a very mild clinical phenotype. Here we might speculate that additional variants in the genetic background of the patient affected their phenotype.

In conclusion, we performed the functional characterization of 14 *CLCN7* mutations found in a cohort of osteopetrotic patients. A critical analysis of clinical and functional data suggests that the lack of CIC-7/Ostm1 complex localization on the lysosomal membrane is involved in the pathogenesis of a specific clinical feature, ie, neurodegeneration, which cannot be rescued by HSCT, as documented in pt 2b. Accordingly, this defect was absent in patients in this cohort bearing mutations that maintained correct membrane targeting, despite abolished transport activity in some cases. Further variants will need to be investigated to strengthen this hypothesis. Further investigations of a larger number of CIC-7 missense mutations, possibly including additional functional read-outs and extensive information regarding the patients' genetic background, will increase the available data set in order to identify structural criteria that can predict confidently the level of pathogenicity. Moreover, the implementation of a database integrating clinical and genetic data of patients, and structural and functional information of mutants, might be useful in guiding treatment decisions in a future perspective. Our study may lay the basis for a specific targeted medicine. Most important for the clinical perspective is that ARO patients without neurodegeneration are candidates for curative HSCT. Moreover, a classical gene-therapy approach could be developed, based on promising results in another subset of osteopetrosis.^(56–58) Mutation-specific approaches might constitute an additional valid alternative. For example, we speculate that CIC-7 mutations leading to faster gating kinetics can be considered gain-of-function mutations to some extent, and we

hypothesize that they may be effectively targeted by siRNA-mediated silencing. Of note, this kind of strategy is being implemented with respect to ADO2⁽¹⁶⁾ and likewise might be pursued in selected ARO patients. On the other hand, for patients with neurodegeneration, HSCT is not indicated because despite rescuing the bone marrow-related pathology, it has no effect on progressive neurological deterioration.⁽⁵⁹⁾

With respect to mutations hampering CIC-7/Ostm1 complex localization on the lysosomal membrane, an intriguing strategy might be represented by pharmacological chaperone therapy (PCT), an emerging approach actively investigated in the field of lysosomal storage disorders (LSDs).⁽⁶⁰⁾ PCT exploits small-molecule ligands to improve lysosomal trafficking and activity of a specific target; therefore, it might also be tested to improve CIC-7/Ostm1 complex localization, possibly loading chaperones on extracellular vesicles or nanoparticles for targeted delivery. Overall, these strategies deserve further investigation.

Disclosures

All authors state that they have no conflicts of interest.

Acknowledgments

We are grateful to the affected individuals and their families for their cooperation. We thank Dr M Pusch for the Ostm1-2AP-CIC-7^{PM}-E²GFP/DsRed-pFrog, CIC-7-pFrog, and Ostm1-pFrog clones; Dr D Arosio for the original E²GFP/DsRed clone; Dr E Lingueglia for the FaNaCh clone; and F Quartino and D Magliozzi for technical assistance. The authors thank Lauren Dreyer, Nurse Coordinator, Undiagnosed Diseases Program, Genetic Services WA, for providing updated clinical information on patient 7. The study was supported by a Telethon Career Award to AP, Assistant Telethon Scientist at the Dulbecco Telethon Institute (TCP 14008, Telethon, Italy).

Authors' roles: The study was conceived and designed by AP, AV, and CS with contribution of EDZ and EP. AP, EDZ, LL, and AR performed research. MA, LDS, BM, JB, JB, AK, SB, GB, FG, MAP, IDM, MRA, RC, and CPB provided clinical information. CS, EP, and DS collected clinical data and performed genetic analysis. AP and CS wrote the manuscript with the contribution of EDZ and EP. All authors revised and approved the manuscript.

Author contributions: EDZ: Data curation; formal analysis; investigation; writing-original draft. EP: Data curation; formal analysis; writing-original draft. LL: Investigation. DS: Data curation. AR: Investigation. MA: Resources. LDS: Resources. BM: Resources. JB: Resources. AK: Resources. SB: Resources. FG: Resources. MAP: Resources. IDM: Resources. MRA: Resources. RC: Resources. CPB: Resources. AV: Conceptualization; supervision; writing-original draft; writing-review and editing. CS: Conceptualization; data curation; formal analysis; supervision; writing-original draft; writing-review and editing. AP: Conceptualization; data curation; formal analysis; funding acquisition; supervision; writing-original draft; writing-review and editing.

PEER REVIEW

The peer review history for this article is available at <https://publons.com/publon/10.1002/jbmr.4200>.

References

1. Teti A. Bone development: overview of bone cells and signaling. *Curr Osteoporos Rep.* 2011;9(4):264–73.
2. Qin A, Cheng TS, Pavlos NJ, Lin Z, Dai KR, Zheng MH. V-ATPases in osteoclasts: structure, function and potential inhibitors of bone resorption. *Int J Biochem Cell Biol.* 2012;44(9):1422–35.
3. Jentsch TJ, Pusch M. CLC chloride channels and transporters: structure, function, physiology, and disease. *Physiol Rev.* 2018;98(3):1493–590.
4. Graves AR, Curran PK, Smith CL, Mindell JA. The Cl^-/H^+ antiporter CIC-7 is the primary chloride permeation pathway in lysosomes. *Nature.* 2008;453(7196):788–92.
5. Lange PF, Wartosch L, Jentsch TJ, Fuhrmann JC. CIC-7 requires Ostm1 as a beta-subunit to support bone resorption and lysosomal function. *Nature.* 2006;440(7081):220–3.
6. Kornak U, Kasper D, Bösl MR, et al. Loss of the CIC-7 chloride channel leads to osteopetrosis in mice and man. *Cell.* 2001;104(2):205–15.
7. Bollerslev J, Henriksen K, Nielsen MF, Brixen K, Van Hul W. Autosomal dominant osteopetrosis revisited: lessons from recent studies. *Eur J Endocrinol.* 2013;169(2):R39–57.
8. Pangrazio A, Pusch M, Caldana E, et al. Molecular and clinical heterogeneity in CLCN7-dependent osteopetrosis: report of 20 novel mutations. *Hum Mutat.* 2010;31(11):E1071–80.
9. Stepensky P, Grisariu S, Avni B, et al. Stem cell transplantation for osteopetrosis in patients beyond the age of 5 years. *Blood Adv.* 2019;3(6):862–8.
10. Teti A, Econs MJ. Osteopetroses, emphasizing potential approaches to treatment. *Bone.* 2017;102:50–9.
11. Palagano E, Menale C, Sobacchi C, Villa A. Genetics of osteopetrosis. *Curr Osteoporos Rep.* 2018;16(1):13–25.
12. Penna S, Capo V, Palagano E, Sobacchi C, Villa A. One disease, many genes: implications for the treatment of osteopetroses. *Front Endocrinol.* 2019;10:85.
13. Waguespack SG, Hui SL, Dimeglio LA, Econs MJ. Autosomal dominant osteopetrosis: clinical severity and natural history of 94 subjects with a chloride channel 7 gene mutation. *J Clin Endocrinol Metab.* 2007;92(3):771–8.
14. Frattini A, Pangrazio A, Susani L, et al. Chloride channel CLCN7 mutations are responsible for severe recessive, dominant, and intermediate osteopetrosis. *J Bone Miner Res.* 2003;18(10):1740–7.
15. Waguespack SG, Koller DL, White KE, et al. Chloride channel 7 (CLCN7) gene mutations and autosomal dominant osteopetrosis, type II. *J Bone Miner Res.* 2003;18(8):1513–8.
16. Maurizi A, Capulli M, Patel R, Curle A, Rucci N, Teti A. RNA interference therapy for autosomal dominant osteopetrosis type 2. Towards the preclinical development. *Bone.* 2018;110:343–54.
17. Leisle L, Ludwig CF, Wagner FA, Jentsch TJ, Stauber T. CIC-7 is a slowly voltage-gated $2\text{Cl}^-/1\text{H}^+$ -exchanger and requires Ostm1 for transport activity. *EMBO J.* 2011;30(11):2140–52.
18. Cleiren E, Benichou O, Van Hul E, et al. Albers-Schonberg disease (autosomal dominant osteopetrosis, type II) results from mutations in the CLCN7 chloride channel gene. *Hum Mol Genet.* 2001;10(25):2861–7.
19. Kang S, Kang YK, Lee JA, Kim DH, Lim JS. A case of autosomal dominant osteopetrosis type 2 with a CLCN7 gene mutation. *J Clin Res Pediatr Endocrinol.* 2019;11(4):439–43.
20. Zhang X, Wei Z, He J, Wang C, Zhang Z. Novel mutations of CLCN7 cause autosomal dominant osteopetrosis type II (ADOII) and intermediate autosomal recessive osteopetrosis (ARO) in seven Chinese families. *Postgrad Med.* 2017;129(8):934–42.
21. Plagnol V, Curtis J, Epstein M, et al. A robust model for read count data in exome sequencing experiments and implications for copy number variant calling. *Bioinformatics.* 2012;28(21):2747–54.
22. Vu TK, Hung DT, Wheaton VI, Coughlin SR. Molecular cloning of a functional thrombin receptor reveals a novel proteolytic mechanism of receptor activation. *Cell.* 1991;64(6):1057–68.
23. Trichas G, Begbie J, Srinivas S. Use of the viral 2A peptide for bicistronic expression in transgenic mice. *BMC Biol.* 2008;6:40.
24. Arosio D, Ricci F, Marchetti L, Gualdani R, Albertazzi L, Beltram F. Simultaneous intracellular chloride and pH measurements using a GFP-based sensor. *Nat Methods.* 2010;7(7):516–8.
25. Dunn KW, Kamocka MM, McDonald JH. A practical guide to evaluating colocalization in biological microscopy. *Am J Physiol Cell Physiol.* 2011;300(4):C723–42.
26. Maurizi A, Capulli M, Curle A, et al. Extra-skeletal manifestations in mice affected by Clcn7-dependent autosomal dominant osteopetrosis type 2 clinical and therapeutic implications. *Bone Res.* 2019;7:17.
27. Zeng B, Li R, Hu Y, et al. A novel mutation and a known mutation in the CLCN7 gene associated with relatively stable infantile malignant osteopetrosis in a Chinese patient. *Gene.* 2016;576(1 Pt 1):176–81.
28. Zheng H, Zhang Z, He JW, Fu WZ, Wang C, Zhang ZL. Identification of two novel CLCN7 gene mutations in three Chinese families with autosomal dominant osteopetrosis type II. *Joint Bone Spine.* 2014;81(2):188–9.
29. Dutzler R, Campbell EB, MacKinnon R. Gating the selectivity filter in CIC chloride channels. *Science.* 2003;300(5616):108–12.
30. Dutzler R, Campbell EB, Cadene M, Chait BT, MacKinnon R. X-ray structure of a CIC chloride channel at 3.0 Å reveals the molecular basis of anion selectivity. *Nature.* 2002;415(6869):287–94.
31. Feng L, Campbell EB, Hsiung Y, MacKinnon R. Structure of a eukaryotic CLC transporter defines an intermediate state in the transport cycle. *Science.* 2010;330(6004):635–41.
32. Park E, Campbell EB, MacKinnon R. Structure of a CLC chloride ion channel by cryo-electron microscopy. *Nature.* 2017;541(7638):500–5.
33. Park E, MacKinnon R. Structure of the CLC-1 chloride channel from *Homo sapiens*. *Elife.* 2018;7:e36629.
34. Wang K, Preisler SS, Zhang L, et al. Structure of the human CIC-1 chloride channel. *PLoS Biol.* 2019;17(4):e3000218.
35. Chen MF, Chen TY. Side-chain charge effects and conductance determinants in the pore of CIC-0 chloride channels. *J Gen Physiol.* 2003;122(2):133–45.
36. Engh AM, Maduke M. Cysteine accessibility in CIC-0 supports conservation in the CIC intracellular vestibule. *J Gen Physiol.* 2005;125(6):601–17.
37. Estevez R, Schroeder BC, Accardi A, Jentsch TJ, Pusch M. Conservation of chloride channel structure revealed by an inhibitor binding site in CIC-1. *Neuron.* 2003;38(1):47–59.
38. Picollo A, Liantonio A, Didonna MP, Elia L, Camerino DC, Pusch M. Molecular determinants of differential pore blocking of kidney CLC-K chloride channels. *EMBO Rep.* 2004;5(6):584–9.
39. Schrecker M, Korobenko J, Hite RK. Cryo-EM structure of the lysosomal chloride-proton exchanger CLC-7 in complex with OSTM1. *Elife.* 2020;9:e59555.
40. Zhang S, Liu Y, Zhang B, et al. Molecular insights into the human CLC-7/Ostm1 transporter. *Sci Adv.* 2020;6(33):eabb4747.
41. Stauber T, Jentsch TJ. Sorting motifs of the endosomal/lysosomal CLC chloride transporters. *J Biol Chem.* 2010;285(45):34537–48.
42. Zanardi I, Zifarelli G, Pusch M. An optical assay of the transport activity of CIC-7. *Sci Rep.* 2013;3:1231.
43. Weinert S, Jabs S, Hohensee S, Chan WL, Kornak U, Jentsch TJ. Transport activity and presence of CIC-7/Ostm1 complex account for different cellular functions. *EMBO Rep.* 2014;15(7):784–91.
44. Weinert S, Jabs S, Supancharat C, et al. Lysosomal pathology and osteopetrosis upon loss of H^+ -driven lysosomal Cl^- accumulation. *Science.* 2010;328(5984):1401–3.
45. Scheel O, Zdebek A, Lourdel S, Jentsch T. Voltage-dependent electrogenic chloride/proton exchange by endosomal CLC proteins. *Nature.* 2005;436:424–7.
46. Benichou J. A review of adjusted estimators of attributable risk. *Stat Methods Med Res.* 2001;10(3):195–216.
47. Ludwig CF, Ullrich F, Leisle L, Stauber T, Jentsch TJ. Common gating of both CLC transporter subunits underlies voltage-dependent activation of the $2\text{Cl}^-/1\text{H}^+$ exchanger CIC-7/Ostm1. *J Biol Chem.* 2013;288(40):28611–9.
48. Sartelet A, Stauber T, Coppieters W, et al. A missense mutation accelerating the gating of the lysosomal Cl^-/H^+ -exchanger CIC-7/Ostm1

- causes osteopetrosis with gingival hamartomas in cattle. *Dis Model Mech.* 2014;7(1):119–28.
49. Nicoli ER, Weston MR, Hackbarth M, et al. Lysosomal storage and albinism due to effects of a de novo CLCN7 variant on lysosomal acidification. *Am J Hum Genet.* 2019;104(6):1127–38.
 50. Astaburuaga R, Quintanar Haro OD, Stauber T, Religio A. A mathematical model of lysosomal ion homeostasis points to differential effects of cl(–) transport in Ca(2+) dynamics. *Cell.* 2019;8(10):1263.
 51. Chalhoub N, Benachenhou N, Rajapurohitam V, et al. Grey-lethal mutation induces severe malignant autosomal recessive osteopetrosis in mouse and human. *Nat Med.* 2003;9(4):399–406.
 52. Heraud C, Griffiths A, Pandravadra SN, Kilimann MW, Pata M, Vacher J. Severe neurodegeneration with impaired autophagy mechanism triggered by OSTM1 deficiency. *J Biol Chem.* 2014;289(20):13912–25.
 53. Pangrazio A, Poliani PL, Megarbane A, et al. Mutations in OSTM1 (grey lethal) define a particularly severe form of autosomal recessive osteopetrosis with neural involvement. *J Bone Miner Res.* 2006;21(7):1098–105.
 54. Prinetti A, Rocchetta F, Costantino E, et al. Brain lipid composition in grey-lethal mutant mouse characterized by severe malignant osteopetrosis. *Glycoconj J.* 2009;26(6):623–33.
 55. Schulz P, Werner J, Stauber T, Henriksen K, Fendler K. The G215R mutation in the cl-/H+-antiporter CLC-7 found in ADO II osteopetrosis does not abolish function but causes a severe trafficking defect. *PLoS One.* 2010;5(9):e12585.
 56. Capo V, Penna S, Merelli I, et al. Expanded circulating hematopoietic stem/progenitor cells as novel cell source for the treatment of TCIRG1 osteopetrosis. *Haematologica.* Epub ahead of print. Available at: <https://doi.org/10.3324/haematol.2019.238261>.
 57. Lofvall H, Rothe M, Schambach A, Henriksen K, Richter J, Moscatelli I. Hematopoietic stem cell-targeted neonatal gene therapy with a clinically applicable lentiviral vector corrects osteopetrosis in oc/oc mice. *Hum Gene Ther.* 2019;30(11):1395–404.
 58. Xian X, Moraghebi R, Lofvall H, et al. Generation of gene-corrected functional osteoclasts from osteopetrotic induced pluripotent stem cells. *Stem Cell Res Ther.* 2020;11(1):179.
 59. Steward CG. Neurological aspects of osteopetrosis. *Neuropathol Appl Neurobiol.* 2003;29(2):87.
 60. Parenti G, Andria G, Valenzano KJ. Pharmacological chaperone therapy: preclinical development, clinical translation, and prospects for the treatment of lysosomal storage disorders. *Mol Ther.* 2015;23(7):1138–48.